

# Electron Spin Resonance

Michael Schmid\* and Henri Menke†  
 Gruppe M05, Fortgeschrittenenpraktikum, University of Stuttgart  
 (November 10, 2014)

The present experiment is mainly divided in two parts. At first we want to characterise the modes of a reflex klystron, record the characteristic curve of the detector diode and measure the standing wave ratio for different experimental adaptations. Second we calibrate the magnetic field of the experimental implementation of the electron spin resonance (ESR). Thereafter we investigate the ESR spectrum of different probes and the hyperfine structure of  $\text{Mn}^{2+}$  and DPPH. Especially we want to determine the Landé  $g$ -factors of  $\text{Cu}^{2+}$  and  $\text{Mn}^{2+}$  and analyse the spin-exchange in TEMPO solutions.

## BASICS

To understand why we need microwaves in this experiment let us look at the level splitting of an electron. The splitting energy is given by  $\Delta E = g_e \mu_B B_{\text{res}}$  and is equivalent to the applied electromagnetic wave  $h\nu$ . It follows that  $\nu = g_e \mu_B B_{\text{res}}/h$  which is roughly 9 GHz for reasonable fields of about 300 mT.

### Microwaves

Electromagnetic waves in the range from 1 GHz to 300 GHz (corresponding to a wavelength of 30 cm to 1 mm) are called *microwaves*. In everyday life microwaves are present in mobile communication such as WiFi, operating at 2.4 GHz and 5 GHz (since 2013), and radar engineering. Before we discuss the generation of microwaves we repeat some basics of electrodynamics to better understand propagation and refraction of microwaves.

#### *Maxwell's Equations*

To describe electromagnetic waves in vacuum it is necessary to know the fundamental equations of electrodynamics

$$\nabla \cdot \mathbf{B} = 0 \quad (1)$$

$$\nabla \cdot \mathbf{E} = \frac{\rho}{\varepsilon_0} \quad (2)$$

$$\nabla \times \mathbf{E} = -\partial_t \mathbf{B} \quad (3)$$

$$\nabla \times \mathbf{B} = \mu_0 \mathbf{j} + \mu_0 \varepsilon_0 \partial_t \mathbf{E} \quad (4)$$

the Maxwell equations. Here  $\mathbf{B}$  ( $\mathbf{E}$ ) is the magnetic (electric) field,  $\rho$  the charge density,  $\mathbf{j}$  the current density,  $\varepsilon_0$  the permittivity of free space, and  $\mu_0$  the permeability of free space. Equation (1) allows to find a vector potential  $\mathbf{A}$  that fulfils  $\mathbf{B} = \nabla \times \mathbf{A}$  (see vector calculus). With help of equation (3) and the vector potential we can ensure the existence of a scalar potential  $\phi$  with  $-\nabla\phi = \mathbf{E} + \partial_t \mathbf{A}$ .

With help of the Lorenz gauge condition

$$\nabla \cdot \mathbf{A} - \varepsilon_0 \mu_0 \partial_t \phi = 0 \quad (5)$$

and the help of equation (4) it is possible to identify wave equations for the potentials

$$\left( \Delta - \frac{1}{c^2} \partial_t^2 \right) \phi = \sqrt{\frac{\mu_0}{\varepsilon_0}} \rho, \quad (6)$$

$$\left( \Delta - \frac{1}{c^2} \partial_t^2 \right) \mathbf{A} = \mu_0 \mathbf{j}. \quad (7)$$

Using the D'Alembert operator and the covariant formulation of electrodynamics allows to find a much more beautiful form of Maxwell's equations, namely

$$\partial_\mu \partial^\mu A^\nu = \mu_0 j^\nu, \quad (8)$$

where  $A^\mu = (\phi/c, \mathbf{A})$  and  $j^\mu = (c\rho, \mathbf{j})$  are four-vectors.

It is an easy exercise to determine the wave equation for  $\mathbf{E}$  in vacuum

$$\square \mathbf{E} = 0. \quad (9)$$

The solution for electric waves in vacuum are plane waves

$$\mathbf{E}(\mathbf{r}, t) = \mathbf{E}_0 e^{i(\mathbf{k} \cdot \mathbf{r} - \omega t)} \quad (10)$$

with der dispersion relation  $\omega = c|\mathbf{k}|$ . If we want to solve Maxwell's equation in waveguides we have to observe additional boundary conditions.

#### *Generation of Microwaves*

To generate electromagnetic waves of any kind in a controlled way a cavity is needed. A cavity has the advantage that we can precisely control which modes of a wave we get. Furthermore, a switch between continuous wave and pulsed wave can be achieved using a cavity. Here we will only use continuous wave, though. There are two kinds of cavities for the generation of microwaves which are presented in the following: The two chamber klystron and the reflex klystron.

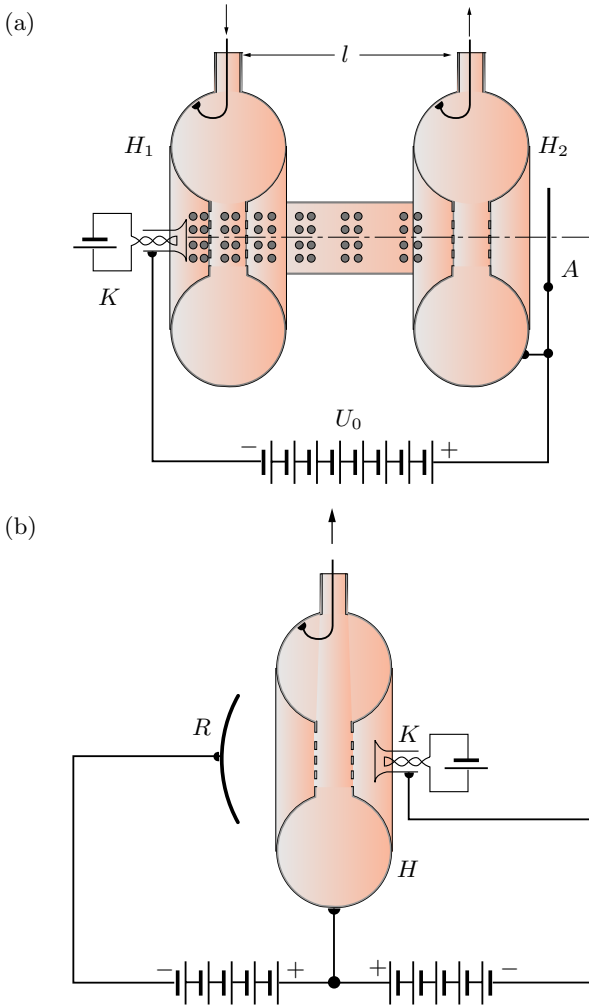


FIG. 1. (a) Sketch of a two chamber klystron, taken from [1, p. 479]. Electrons are generated at the cathode  $K$  and accelerated by a positively charged slit. The resonator  $H_1$  applies a velocity modulation, resonator  $H_2$  a density modulation. The backcoupling of both allows usage as cavity. (b) Sketch of a reflex klystron, also taken from [1, p. 479]. Electrons are again generated at the cathode  $K$  and accelerated by a slit but then reflected by the repeller  $R$ . This results in a reversal of the direction of flight and, if the repeller voltage was chosen appropriately, in a resonant mode in the cavity. In this experiment we use a reflex klystron.

*Two Chamber Klystron:* A sketch of a two chamber klystron can be viewed in figure 1 a). A hot cathode emits electrons that are accelerated by a positively charged slit to energies in the range of several keV. The electron beam enters the first chamber  $H_1$ . The electric field present in  $H_1$  accelerated or slows down the electrons depending on their velocity. This velocity modulation leads to formation of clusters with electrons of the same speed, which can be viewed as a density modulation. The second chamber is placed at the maximum of the density amplitude where this oscillation produces a voltage in the walls of the

chamber with the same frequency as the mode in the first chamber. The frequency depends on the geometry of the resonator and can thus not be influenced easily.

*Reflex Klystron:* A sketch of a reflex klystron is depicted in figure 1 b). A reflex klystron only consists of one resonator. Instead of the second resonator there is a reflector electrode, which is negatively charged. During the slowing down and accelerating in the opposite direction a density modulation emerges. During the second pass through the resonator the electrons exchange energy with the resonator field. Only if the electrons have the correct velocity on reentering of the cavity (determined by  $U_R$ ) they provide energy to the field by slowing down, else they absorb energy from the field to accelerate.

### Microwaves in waveguides

Every linear structure that conveys electromagnetic waves is called waveguide. The waveguides used in the experiment are hollow metal pipes. With the help of Maxwell's equations and boundary conditions determined by the properties of the materials it is possible to analyse the behaviour of microwaves in waveguides and identify the possible modes. Henceforth the waveguide is assumed to be aligned in  $z$ -direction. Electromagnetic waves propagating in waveguides are reflected on the walls and form standing waves leading to a discrete spectrum of allowed modes.

To identify the possible modes it is necessary to solve the wave equation (9). Due to the alignment of the waveguide we use the ansatz

$$\mathbf{E}(\mathbf{r}, t) = \mathbf{E}_0(x, y) \cos(\omega t - k_z z) \quad (11)$$

which yields

$$\partial_x^2 \mathbf{E} + \partial_y^2 \mathbf{E} + \left( \frac{\omega}{c^2} - k_z^2 \right) \mathbf{E} = 0. \quad (12)$$

The boundary conditions in waveguides demand a vanishing tangential component of  $\mathbf{E}$  on the walls (von Neumann condition). This implies that the electric field  $\mathbf{E}$  is always perpendicular to the magnetic field  $\mathbf{B}$  which is therefore orientated tangentially to the conductive walls. This conditions are fulfilled if

$$k_x = \frac{\pi n}{a}, \quad k_y = \frac{\pi m}{b} \quad (13)$$

and  $n, m \in \mathbb{N}$ . The constants  $a$  and  $b$  describe the width and height of the waveguide. Using Maxwell's equations we identify:

*TE-Modes:* Solutions that have no electric field in the direction of propagation ( $\mathbf{E} \perp \mathbf{e}_z$ ) are called transverse electric modes.

*TM-Modes:* Solutions that have no magnetic field in the direction of propagation ( $\mathbf{B} \perp \mathbf{e}_z$ ) are called transverse magnetic modes.

*TEM-Modes:* Transverse electromagnetic modes have neither an electric field nor a magnetic field component in the direction of propagation. Due to Maxwell's equations these solutions are not possible in hollow waveguides. However TEM-modes can propagate in coaxial cables or free space.

To investigate the dispersion in hollow waveguides we use  $\omega = ck$  and the conditions (13)

$$\begin{aligned} k_z &= \sqrt{\frac{\omega^2}{c^2} - \pi \left( \frac{n^2}{a^2} + \frac{m^2}{b^2} \right)} \\ &= \sqrt{k^2 - k_g^2}. \end{aligned} \quad (14)$$

An undamped propagation in  $z$ -direction is only possible if the threshold wavelength  $\lambda_g = 2\pi/k_g$  is greater than the wavelength of the electromagnetic wave  $\lambda$  or  $k_g \geq k$ . The threshold wavelength is therefore given by

$$\lambda_g = 2 \left( \frac{n^2}{a^2} + \frac{m^2}{b^2} \right)^{-1/2}. \quad (15)$$

To compare the vacuum wavelength  $\lambda_v = c/\nu$  with  $\lambda_g$  it is common to define an effective wavelength

$$\lambda_e \equiv \frac{2\pi}{k_z} = \lambda_v \left( 1 - \frac{\lambda_v^2}{\lambda_g^2} \right)^{-1/2}. \quad (16)$$

Obviously the wavelength of electromagnetic waves in hollow waveguides is greater than the wavelength of an electromagnetic waves of the same frequency in vacuum.

*Standing Waves:* A standing wave is caused by the interference of two waves propagating in opposite directions (e.g. interference between an incoming and a reflected wave). The two waves are described by

$$\mathbf{E}_i(\mathbf{r}, t) = \mathbf{E}_0 \cos(\omega t - kz) \quad (17)$$

$$\mathbf{E}_r(\mathbf{r}, t) = \mathbf{E}_0 \cos(\omega t + kz). \quad (18)$$

The interference of both waves is

$$\begin{aligned} \mathbf{E}(\mathbf{r}, t) &= \mathbf{E}_i(\mathbf{r}, t) + \mathbf{E}_r(\mathbf{r}, t) \\ &= 2\mathbf{E}_0 \sin(kz) \cos(\omega t) \end{aligned} \quad (19)$$

where we used some trigonometric identities. This function of a standing wave is characterised by its nodes and antinodes. The gifted reader might have noticed that for standing waves it is not possible to transport energy and therefore they are impractical for our experiment.

#### Reflection of Waves

When a wave hits the end of a waveguide, whatever boundary condition applies, it is reflected. This is not a hard reflection where 100 % of the wave are scattered backwards, but a transition from a regime of a first impedance

$Z_1$  into a regime of another impedance  $Z_2$ . In general the impedance depends on the position inside the waveguide, i.e.,  $Z = Z(\mathbf{r})$ . For the vacuum we find  $Z_{\text{vac}} = \sqrt{\mu_0/\epsilon_0}$ . For the transition  $Z_1 \rightarrow Z_2$  we find the *reflection coefficient*

$$p = \frac{E^{(r)}}{E^{(i)}} = \frac{Z_2 - Z_1}{Z_2 + Z_1}$$

The indices  $^{(r)}$  und  $^{(i)}$  stand for für reflected and incident, respectively. The reflection coefficient is  $p = 0$  if  $Z_2 = Z_1$ . Therefore open end waveguides are capped by a terminal resistance. To keep the reflection factor small one tries to smoothly transfer waves from one guide to another, in the case of microwaves using so called *horn radiators*.

Reflected waves inside a waveguide lead to (undesired) standing waves, as discussed above. Those standing waves are in most cases not completely stationary, but are superimposed with propagating parts. To quantify the amount of superposition one defines the *standing wave ratio* (SWR) as the ratio of maximum and minimum electric field amplitude

$$\text{SWR} \equiv \frac{E_{\text{max}}}{E_{\text{min}}} = \frac{|E_1^{(i)}| + |E_1^{(r)}|}{|E_1^{(i)}| - |E_1^{(r)}|} = \frac{1 + |p|}{1 - |p|} \quad (20)$$

with the just introduced reflection coefficient  $p$ . There are two limit cases worth mentioning:  $\text{SWR} = 1 \iff |p| = 0$  corresponds to an ideal setup as there is no reflection at all, whereas  $\text{SWR} = \infty \iff |p| = 1$  resembles the worst case of total reflection, i.e. standing waves inside the waveguide.

#### Determining the SWR

There are three different techniques to determine the SWR in a hollow waveguide, which are all presented in the following. All of the are based on the insertion of a probe into the waveguide.

*Interlude on Damping:* To quantify ratios using the *Decibel scale* one computes the logarithm of the ratio to base ten and multiplies the result with ten. Hence, 10 dB corresponds to a tenfold increase, whereas 3 dB approximately describes a doubling and 3 dB a halving. Formally one has

$$\begin{aligned} L(E_1, E_2) &= 10 \log_{10} \left( \frac{E_1^2}{E_2^2} \right) \text{dB} \\ &= 20 \log_{10} \left( \frac{E_1}{E_2} \right) \text{dB} \\ &= 2 \log_{10} \left( \frac{E_1}{E_2} \right) \text{B} \end{aligned}$$

Because the damping takes place over the whole extent of the waveguide, it is common to put it in relation to that. In most cases this is dB/10 m or dB/100 m.

*The SWR metre method:* This method is reliable for small to medium SWR. The procedure is as follows:

1. We insert the probe into the waveguide and move it to the location of maximum amplitude (if there is none, we immediately conclude  $\text{SWR} = 1$ ).
2. We note down the damping shown on the SWR metre as  $L_{\max}$ .
3. The probe is moved towards the amplitude minimum.
4. We note down the damping shown on the SWR metre as  $L_{\min}$ .
5. The SWR can be calculated by the formula

$$\text{SWR} = \frac{E_{\max}}{E_{\min}} = 10^{\frac{L_{\min} - L_{\max}}{20 \text{ dB}}} \quad (21)$$

*The 3 dB method:* In contrast to the SWR metre method we can measure large SWR with this method.

1. We insert the probe into the waveguide and move it to the location of minimum amplitude (if there is none, we immediately conclude  $\text{SWR} = 1$ ).
2. We note down the damping shown on the SWR metre as  $L_{\min}$ .
3. The probe is moved to the left and to the right, successively, to a damping of  $L = L_{\min} - 3 \text{ dB}$ .
4. We note down the positions of the probe as  $d_l$  and  $d_r$ .
5. We determine the wavelength  $\lambda_g$  in the waveguide by, e.g. taking the distance of two minima.
6. The SWR can be calculated by the formula

$$\text{SWR} = \sqrt{1 + \frac{1}{\sin^2\left(\frac{\pi(d_l - d_r)}{\lambda_g}\right)}} \approx \frac{\lambda_g}{\pi(d_l - d_r)} \quad (22)$$

*The attenuator method:* Because we use this method to measure really large SWR we need to plug an attenuator between the klystron and the measurement diode to prevent an overload.

1. We insert the probe into the waveguide and move it to the location of minimum amplitude (if there is none, we immediately conclude  $\text{SWR} = 1$ ).
2. The attenuator is set to  $L_{\min} = 20 \text{ dB}$ , the amplification of the SWR metre is set, such that it shows a damping of 3 dB.
3. Now we move the probe towards a (relative) maximum amplitude, while making sure to adjust the attenuator in such a way that we do not cause an overload.

4. The attenuator is set to a value  $L_{\max}$ , such that the SWR metre shows a damping of 3 dB (as before).
5. The SWR can be calculated by the formula

$$\text{SWR} = 10^{\frac{L_{\max} - L_{\min}}{20 \text{ dB}}} \quad (23)$$

## Electron Spin Resonance

Electron spin resonance (ESR) is a phenomenon similar to nuclear magnetic resonance (NMR). It is based on transitions between adjacent levels of electrons in an external magnetic field. These transitions can be induced by stimulation with microwaves and thus give rise to characteristic resonance spectra.

### *Electron and Spin*

Electrons have a property called *spin* that make them able to interact with a magnetic field. The spin can be motivated by quantum field theories. Namely, the Dirac equations has two solutions of positive energy and two of negative energy. This twofold characteristic is then defined to be the spin. Nevertheless, the spin was discovered long before it was postulated, by the Stern-Gerlach experiments. Nowadays the standard model assigns a spin of  $S = 1/2$  to the electron, because it is a fermion (like all hadrons). The spin can be connected to a magnetic moment

$$\boldsymbol{\mu} = \gamma \mathbf{S} \quad (24)$$

where  $\gamma$  is the gyromagnetic ratio, which can be expressed in terms of the Landé- $g$ -factor (see below)

$$\gamma = g \frac{\mu_B}{\hbar} \quad (25)$$

where  $\mu_B$  is the Bohr magneton and  $\hbar$  the Planck constant.

The quantum mechanics of angular momenta states the commutation relation  $[S_i, S_j] = i\epsilon_{ijk} S_k$  for a vector operator  $\mathbf{S}$ . The eigenstates are given in terms of two quantum numbers  $s$  and  $m_s$ .

$$\mathbf{S}^2 |s, m_s\rangle = \hbar^2 s(s+1) |s, m_s\rangle$$

$$S_z |s, m_s\rangle = \hbar m_s |s, m_s\rangle$$

where  $m_s \in \{-s, \dots, s\}$ . Now the spin is fully described by its  $z$  component  $S_z$  and its modulus squared  $\mathbf{S}^2$ . This allows for a representation in the vector model, c.f. figure 2 (b).

### *Interaction with the Electromagnetic Field*

With the knowledge of the previous section we obtain for the magnetic moment

$$\boldsymbol{\mu} = |\boldsymbol{\mu}| = \gamma |\mathbf{S}| = \sqrt{s(s+1)} \mu_B g_e \quad (26)$$

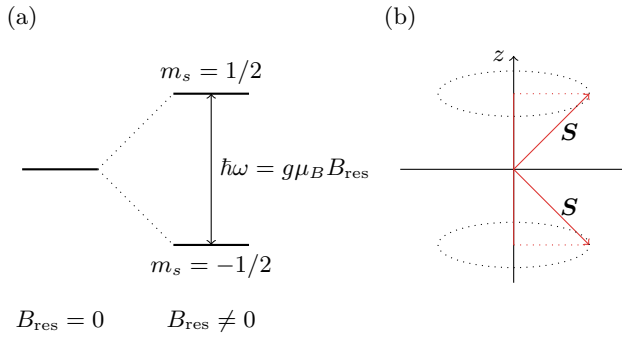


FIG. 2. (a) Energy levels of an electron in absence and presence of a magnetic field  $B$ . The two possible spin states  $m_s = \pm 1/2$  lose their degeneracy in presence of an external magnetic field. (b) Vector representation of the electron spin. The  $z$  axis is chosen as the quantisation axis.

In presence of the magnetic field  $\mathbf{B}_0$  there are only two possible configurations  $m_s = \pm 1/2$  (magnetic spin quantum number) of the electron. Due to the Zeeman effect (figure 2) each configuration has the specific energy  $E = m_s g_e \mu_B \mathbf{B}_0$ . The energy difference is therefore

$$\Delta E = h\nu = g_e \mu_B \mathbf{B}_0. \quad (27)$$

Equation (27) is also called the fundamental equation of electron spin resonance because if an electromagnetic wave with frequency  $\nu$  is coupled perpendicular to the direction of  $\mathbf{B}_0$  it is possible to observe a transition between the two configurations of the electron spin. This is called electron spin resonance (ESR).

Note that the electron spin resonance is only possible for samples with permanent dipole moment (so called paramagnetic sample).

We now study the interaction of a spin with a time dependent magnetic field, such as a microwave. The interaction term of such a Hamiltonian is given by

$$H = -\boldsymbol{\mu} \cdot \mathbf{B} \quad (28)$$

Let now  $\mathbf{B}(t) = (B \cos \omega t, 0, 0)$ . It follows

$$H = -\frac{g\mu_B}{\hbar} S_x B \cos \omega t \quad (29)$$

Using time dependent perturbation theory and  $S_x = (S_+ + S_-)/2$  we find

$$P_{i \rightarrow f} \sim |\langle f | V | i \rangle|^2 \sim |\langle f | S_+ | i \rangle + \langle f | S_- | i \rangle|^2 \quad (30)$$

which means that the probability for transitions  $|\uparrow\rangle \rightarrow |\downarrow\rangle$  and  $|\downarrow\rangle \rightarrow |\uparrow\rangle$  is non-zero. These processes are called stimulated emission and stimulated absorption.

In the vector model the spin can be treated like a classical angular momentum. A torque  $\mathbf{T}$  towards the magnetic moment leads to the angular momentum  $\mathbf{S}$  to

precess around the axis defined by the magnetic field at the Larmor frequency  $\omega_L$ .

$$\omega_L = \frac{g\mu_B}{|\mathbf{S}|} B = \gamma B$$

When a magnetic field is applied it takes some time for the system to reach the equilibrium state of magnetisation  $M_0$ . The process of approaching this state can be described by a differential equation with the longitudinal relaxation time  $T_1$ . Because the spin exchanges energy with its surroundings (called lattice), this one is called *spin-lattice-relaxation time*. There also exists a transversal magnetisation  $M_x$  and  $M_y$ , which depend on the transversal relaxation time  $T_2$  (spin-spin relaxation time).

If now a magnetic field is applied, which operates near the Larmor frequency, we get the so called *Bloch equations* in the rotating frame.

$$\frac{d}{dt} M_x^* = (\gamma B_0 - \omega) M_y^* - \frac{M_x^*}{T_2} \quad (31a)$$

$$\frac{d}{dt} M_y^* = -(\gamma B_0 - \omega) M_x^* - \gamma B_1 M_z^* - \frac{M_y^*}{T_2} \quad (31b)$$

$$\frac{d}{dt} M_z^* = -\gamma B_1 M_y^* - \frac{M_z^* - M_0}{T_1} \quad (31c)$$

The terms containing the times  $T_1$  and  $T_2$  describes the relaxation process, while the terms containing  $B_0$  describe a precession around the magnetisation  $\mathbf{M}^*$  and the terms with  $B_1$  reflect a movement around the  $x^*$ -axis.

A homogeneous static magnetic field  $\mathbf{B}_0 = B_0 \mathbf{e}_z$  is applied in  $z$  direction. The nuclear spin now precesses around this field. Now a high frequency magnetic pulse  $\mathbf{B}_{\text{HF}}$  is put on, perpendicular to  $\mathbf{B}_0$ , the magnetisation is deflected towards the field resulting from a superposition of  $\mathbf{B}_0$  and  $\mathbf{B}_{\text{HF}}$ .

After this pulse the magnetisation returns to equilibrium as described by the Bloch equations (31,a-c). In the time, when the spin magnetic moment does not precess around  $\mathbf{B}_0$ , an oscillating magnetic field is applied.

The oscillating field is applied in two modes:

- 90°-pulses last the time  $t_W$ , which exactly deflects the spin from its idle state to the  $x, y$ -plane.
- 180°-pulses last for  $2t_W$  and invert the spins.

The time between two pulses is  $\tau$ .

After the 90°-pulse is put in some spins precess faster than others due to inhomogeneities in the field  $\mathbf{B}_0$  and the various magnetic surrounding in the sample itself. Because of the precessions drifting apart we obtain a decaying signal, called FID-Signal (free induction decay). After  $2\tau$  a *spin echo* can be measured because when inverting the spins the precessions start to approach again and when they meet the resonance signal is at a maximum, due to all spins being in phase.

*The Landé  $g$ -factor*

In general the Landé  $g$ -factor isn't a simple scalar. This is only true for free electrons. Because the  $g$ -factor is anisotropic in many crystals it is necessary to introduce a symmetric Tensor  $\mathbf{g}$  which is diagonalisable and has the form

$$\mathbf{g} = \begin{pmatrix} g_{xx} & 0 & 0 \\ 0 & g_{yy} & 0 \\ 0 & 0 & g_{zz} \end{pmatrix}. \quad (32)$$

The directions parallel to the eigenvectors of the eigenbasis are called principal axes.

In many physical problems the  $\mathbf{g}$  Tensor has an additional symmetry that allows  $g_{xx} = g_{yy}$ . Consequently we are able to define two further quantities

$$g_{\parallel} \equiv g_{zz}, \quad (33)$$

$$g_{\perp} \equiv g_{xx} = g_{yy}, \quad (34)$$

that we have to determine in the experiment.

Let  $\mathbf{e}_z$  be the principal axis to  $g_{\parallel}$  of a crystal with axial symmetry to  $\mathbf{e}_x$  and  $\mathbf{e}_y$ . The magnetic field  $\mathbf{B}_0$  can be described with spherical coordinates  $\theta$  and  $\varphi$ . With respect to the additional symmetry  $g_{xx} = g_{yy}$  we can rewrite the Landé  $g$ -factor

$$g(\theta, \varphi) = \sqrt{g_{\perp} \sin^2 \theta + g_{\parallel} \cos^2 \theta}. \quad (35)$$

In the case of  $\mathbf{e}_z \parallel \mathbf{B}_0$  the angle  $\theta = 0$  and  $g = g_{\parallel}$ . Rotating the sample to  $\mathbf{e}_z \perp \mathbf{B}_0$ , which implies  $\theta = \pi/2$ , allows to measure  $g = g_{\perp}$ .

*Hyperfine Structure*

The hyperfine structure of an ESR spectrum, caused by the magnetic interaction of the momenta of neighbouring electrons and nuclei, describes a splitting of ESR resonances of active electrons in multiple lines. The Hamiltonian is then given by

$$\begin{aligned} H &= H_Z + H_{\text{HFS}} \\ &= -g_e \frac{\hbar}{\mu_B} \mathbf{B}_0 \cdot \mathbf{S}_z + \mathbf{S} \mathbf{A} \mathbf{I}, \end{aligned} \quad (36)$$

where  $H_Z$  is the Zeeman interaction and  $\mathbf{A}$  the hyperfine structure tensor. Note that the Hamiltonian (36) only covers the interaction between one electron and one nucleus. To describe the interaction between more electrons and nuclei it is necessary to add some more terms. Only for non-vanishing nuclear spin  $\mathbf{I}$  the observation of hyperfine splitting in ESR spectra is possible. More precisely

$H_{\text{HFS}}$  is given by

$$\begin{aligned} H_{\text{HFS}} &= H_{\text{Dipole}} + H_{\text{Iso}} \\ &= -\frac{\mu_0 g_e \mu_B g_I \mu_I}{3\pi \hbar} \left[ \left[ \frac{2(\mathbf{S} \mathbf{r})(\mathbf{r} \mathbf{I})}{|\mathbf{r}|^5} - \frac{\mathbf{S} \mathbf{r}}{|\mathbf{r}|^3} \right] + \frac{8\pi \delta(\mathbf{r})}{3} \mathbf{S} \mathbf{I} \right], \end{aligned} \quad (37)$$

where terms subscripted with  $I$  belong to the nucleus.

*Dipole Interaction:*  $H_{\text{HFS}}$  describes the dipole interaction which depends on the relative orientation of the vector  $\mathbf{r}$  between electron, nucleus and the external magnetic field  $B_0$ . This anisotropy results in a hyperfine splitting depending on the orientation of the sample in the magnetic field.

*Fermi Contact Interaction:*  $H_{\text{Iso}}$  describes the fermi contact interaction which is the magnetic interaction between an electron and an atomic nucleus where the electron is assumed to be at the position of the nucleus. This interaction is independent of the orientation of the sample in a magnetic field. Therefore this interaction is responsible for the hyperfine splitting in liquid samples. The spin density is then given by  $|\psi(0)|^2$ , where  $\psi(0)$  is the electron wavefunction at the position of the nucleus.

*Spin Exchange*

In liquid ESR samples spin exchange describes a spin diffusion between paramagnetic molecules. It is caused by spin-spin interaction of two ESR active electrons of different molecules. This interaction appears when the orbitals of both electrons overlap. In fluids this is the case for collisions of paramagnetic molecules. The Hamiltonian is then given by

$$H_{SS} = \hbar J(\mathbf{r}) \mathbf{S}_1 \mathbf{S}_2, \quad (38)$$

where  $J(\mathbf{r})$  is the exchange integral. The eigenstates of the Hamiltonian are given by the singlet and the three triplet states. It is an easy task to determine these with the help of the angular momentum algebra. Indeed, the molecules of the fluid are not in entangled states, but in product states  $|\uparrow\uparrow\rangle, |\downarrow\downarrow\rangle$ , etc. The two states of parallel spin are eigenstates of the aforementioned Hamiltonian. During a collision there might be a spin flip. This process is given by

$$A(\uparrow) + B(\downarrow) \rightleftharpoons A(\downarrow) + B(\uparrow). \quad (39)$$

The reaction rate is then given by  $\omega_e = k_e c_A c_B$ , where  $c_A$  and  $c_B$  are the concentrations of species  $A$  and  $B$ , and  $k_e$  is a rate constant.  $k_e$  gives information about the quantum mechanical part of the spin exchange

$$k_e = p k_D. \quad (40)$$

Here  $p$  is the mean efficiency of a collision, and  $k_D$  the diffusion coefficient. Note that  $p$  depends on the exchange

integral  $J$  and the mean collision time  $\tau_c$ . From non-hermitian quantum mechanics (NHQM) it can be derived that the line width of a resonance is proportional to the life time of the corresponding state and hence depends on the kind of spin exchange.

*Slow Spin Exchange:* For slow spin exchange the resonance becomes wider and position shifted.

*Moderate Spin Exchange:* For moderate spin exchange the resonances become one unified resonance.

*Fast Spin Exchange:* For fast spin exchange the width of the unified resonances become narrower.

If there are more resonances in the measured data it is necessary to use a multiple Lorentz-fit

$$\mathcal{L}(\omega) = \frac{\Delta\omega^2}{\omega_e} \frac{I}{\omega^2 + \frac{(\omega^2 - \Delta\omega_2/4)^2}{\omega_e^2}}, \quad (41)$$

where  $\omega$  is the microwave frequency,  $\omega = k_e c$  the exchange rate and  $\Delta\omega$  the distance of the lines if the spectrum only consists of two lines. In the regime of slow spin exchange it is possible to identify a linear dependency between the FWHM  $\Delta B$  of the resonances and the concentration

$$\Delta B(c) - \Delta B(c=0) \propto k_e c. \quad (42)$$

An explicit result is given by

$$k_e c = \frac{g_e \mu_B}{\hbar} \left| \frac{1}{1 - \varphi} \right| (\Delta B(c) - \Delta B(c=0)), \quad (43)$$

where  $\varphi$  is the statistical measure of the investigated resonance. The statistical measure  $\varphi$  is given by the ratio between the number of  $m_I$  configurations of the observed resonance and the number of all possible configurations.

### Spectral Lines

Resonance lines in spectra should in theory be perfect delta peaks, but due to the inevitable interaction with the environment the lines get broadened. This leads to a very important property of spectral lines viz. the line width. In our experiment the absorption curves can be approximated by a Lorentzian

$$\mathcal{L}(B) = \frac{I}{1 + \left(\frac{2}{\Delta B}(B - B_{\text{res}})\right)^2} \quad (44)$$

with the intensity  $I$ , the centre  $B_{\text{res}}$  and the “full width at half maximum” or FWHM  $\Delta B$ .

Because the ESR spectra are recorded using effect modulation of the magnetic field we always measure the derivative of the signal, hence our spectral lines will have the form of a differential Lorentzian.

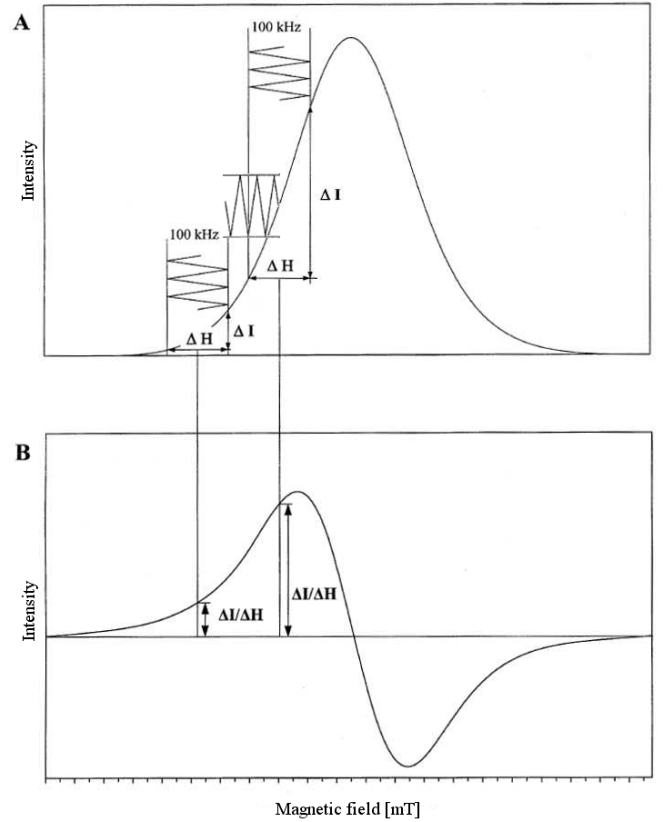


FIG. 3. The intensity amplitude  $\Delta I$  is ejected by the lock-in amplifier. The measured signal is proportional to the derivative of the absorption curve. Taken from [2].

## Experimental Requirements

To measure electron spin resonance certain prerequisites have to be fulfilled and certain devices and techniques are needed. The technique of effect modulation is explained in the following because it is a crucial part for reliably measuring ESR. Also the working principle of a lock-in amplifier is explained. It is needed because the measured signal in the cavity is very noisy and a lock-in amplifier offers methods to smooth it.

### Effect Modulation

Due to the bad signal-to-noise ratio a direct measurement of attenuation of microwaves is not possible. To solve this problem we use a technique called effect modulation. With help of a lock-in amplifier an enhancement of the measured signals are possible.

To do so it is necessary to use additional modulation coils in the resonator with a typical frequency component of 100 kHz. A previous magnetic field in  $z$ -direction is

then modified such that it is given by

$$B(t) = B_{\text{stat}} + \Delta B \left( \frac{t}{t_0} - \frac{1}{2} \right) + \frac{1}{2} B_m \sin(\omega_m t), \quad (45)$$

where  $\omega_m$  is the modulation frequency which is much faster than the linear change of the magnetic field,  $B_m$  the modulation amplitude which is small compared to the width of the resonance and  $\Delta B$  is the measured timeframe, c.f. figure 3. The figure shows that the modulation of the magnetic field also causes a modulation of the absorbed microwave power. Disorders caused by other sources than the ESR absorption of the microwave are not modulated. It is also depicted that the issued voltage of the lock-in amplifier is proportional to the derivative of the absorption curve. The absorption curve is a result of numerical or electronic integration.

#### Lock-In Amplifier

A lock-in amplifier is a technical device used to detect and measure small AC signals down to a few nanovolts. With their help it is possible to extract signals with known carrier waves from noisy environments. Therefore they use a technique known as phase-sensitive detection.

An common lock-in amplifier amplifies and then multiplies the incoming signal

$$U_{\text{sig}} = U_{\text{sig},0} \sin(\omega_{\text{sig}} t + \theta_{\text{sig}}) \quad (46)$$

from an experiment (e.g. an oscillator) with a lock-in reference

$$U_{\text{ref}} = U_{\text{ref},0} \sin(\omega_{\text{ref}} t + \theta_{\text{ref}}), \quad (47)$$

where  $U_{\text{sig},0}$  is the signal amplitude. Note that the reference signal in the experiment is the signal of the magnetic field modulation and the incoming signal is the measured microwave power excited from the magnetic field modulation. Multiplying both signals yield

$$U_M = U_{\text{sig},0} U_{\text{ref},0} \sin(\omega_{\text{sig}} t + \theta_{\text{sig}}) \sin(\omega_{\text{ref}} t + \theta_{\text{ref}}).$$

With the help of some trigonometrical identities we can rewrite the signal

$$U_M = \frac{1}{2} [\tilde{U} \cos((\omega_{\text{sig}} - \omega_{\text{ref}})t + \theta_{\text{sig}} - \theta_{\text{ref}}) - \tilde{U} \cos((\omega_{\text{sig}} + \omega_{\text{ref}})t + \theta_{\text{sig}} + \theta_{\text{ref}})], \quad (48)$$

where  $\tilde{U} = U_{\text{sig},0} U_{\text{ref},0}$ . The signal  $U_M$  is passed through a low pass filter which only let a signal pass if  $\omega_{\text{sig}} = \omega_{\text{ref}}$ , i.e. , the filtered output will be a very nice DC signal

$$U_{\text{Out}} = \frac{1}{2} \tilde{U} \cos(\theta_{\text{sig}} - \theta_{\text{ref}}). \quad (49)$$

To maximise the output signal  $U_{\text{Out}}$  the condition  $(\theta_{\text{sig}} - \theta_{\text{ref}} = 2\pi n$  and  $n \in \mathbb{N}$  has to be fulfilled. This can be achieved with a manual phase shifting device or using a second lock-in amplifier with an  $\pi/2$  phase shifted fix reference signal. Unfortunately in the experimental set-up only a manual phase shifting device is possible.

## ANALYSIS

### Experiments on ESR I

In this section we deal with experiments which are needed in preparation for actual ESR spectra. Important quantities to determine are the  $Q$ -factors of our samples. This can be done without any magnetic field. As all subsequent measurements depend on a magnetic field, which is adjusted via its Hall voltage, we need to calibrate the Hall probe using the well gauged DPPH. Next a set of optimal system parameters is to be found, such that the quality of ESR spectra is maximised with respect to power of the microwave radiation, as well as modulation frequency, Hall voltage, and amplitude of the magnetic field, and ultimately delay time of the lock-in amplifier. Afterwards the first ESR spectra are recorded to analyse the hyperfine structure in DPPH depending on the concentration, and compute the  $g$ -Tensor of  $\text{CuSO}_4$  and  $\text{Mn}^{2+}$ .

#### Experimental Setup

As described in the basics, the experimental setup needs to incorporate several devices for different purposes. First of all we need a reflex klystron to generate microwaves. Then we need an adjustable damping unit and a magical T for backcoupling to the klystron. Finally we have Helmholtz coils.

Each of these devices fulfils a certain purpose. The klystron for instance does not only generate microwaves in an unspecified way, but it uses the signal detected by a diode somewhere else in the circuit to adjust its frequency. The adjustable damping unit is needed because we don't want to record all signals at the same intensity. Some samples need to experience some more power, some need less. The magical T is used to distribute the signal coming from the klystron back to the diode associated with the klystron and to the magnetic field coils. Inside the Helmholtz coils the magnetic field is generated which will lift the degeneracy of the initially degenerate  $m_s$  states by means of a Zeeman interaction.

In one of the upcoming sections we're going to investigate the dependency of the ESR spectra on several system parameters. These include:

- The modulation frequency and amplitude of the magnetic field which can both be adjusted at the power supply of the Helmholtz coils.



FIG. 4. Photo of the experimental setup. Not all components are visible in the picture. The black can on the far left are the Helmholtz coils for the magnetic field. A little right to it we see the magical T. In the middle is the adjustable damping module and on the far left the klystron. The whole setup was much larger and included all sorts of measurement devices and power sources—these are not illustrated.

- The microwave power can be adjusted using the aforementioned damping unit.
- The integration time of the signal can be selected on the lock-in amplifier.

Another free parameter was the magnetic field sweep which was selected on the computer interface, but this had no effect on the actual outcome of the measurement.

#### Quality of the resonator

The quality factor  $Q$  of a resonator characterises the bandwidth relative to its resonance frequency and thus is a dimensionless quantity. We use the definition

$$Q \equiv \frac{\nu_0}{\Delta\nu}, \quad (50)$$

where  $\nu_0$  is the resonance frequency and  $\Delta\nu$  the bandwidth (FWHM). The higher the  $Q$ -factor, the lower are the dissipative losses in the resonator. The investigation of the different samples with ESR extract energy from the modes in the resonator and will lead to a decreasing quality factor.

In the following subsection we want to determine the  $Q$ -factor for an empty resonator and filled resonator with the samples DPPH (poly),  $\text{CuSO}_4$  (poly) and  $\text{Mn}^{2+}$  (aq). To do so, it is necessary to adjust the klystron frequency by modifying the resonator geometry. The goal of this adjustment is to shift the absorption dip of the resonator to the most powerful klystron mode. For this purpose we use an oscilloscope. With help of an additional measurement resonator it is possible to detect the resonator mode. With help of a micrometre we can adjust the position of

TABLE I. Resonator quality  $Q = \nu_0/\Delta\nu$  for different samples. The peak frequency is labelled with  $\nu_0$  and the width (FWHM) with  $\Delta\nu$ . The Position was measured with an micrometer. The positions left and right of the resonance dip are labelled with  $x_l$  and  $x_r$ .

Sample	$x_l$ [mm]	$x_0$ [mm]	$x_r$ [mm]	$\nu_0$ [GHz]	$\Delta\nu$ [kHz]	$Q$ [1]
empty	7.808	7.832	7.848	9.518	5.363	1775
DPPH	7.868	7.888	7.908	9.511	5.326	1786
$\text{CuSO}_4$	7.876	7.896	7.920	9.510	5.852	1625
$\text{Mn}^{2+}$	7.808	7.832	7.852	9.518	5.898	1614

the resonance frequency (minimum)  $x_0$  and the left  $x_l$  and right  $x_r$  position at half maximum. With help of the calibration curve

$$\frac{\nu(x)}{\text{GHz}} = 11.045 - 0.25589 \cdot \frac{x}{\text{mm}} + 0.00778 \cdot \left(\frac{x}{\text{mm}}\right)^2 \quad (51)$$

we can match every measured position to a frequency. To determine the bandwidth we use the formula  $\Delta\nu = |\nu(x_l) - \nu(x_r)|$ . With equation (50) it is possible to find the  $Q$ -factors for each sample. Thereto see table I.

As predicted the  $Q$ -factors of the particular samples are smaller than the  $Q$ -factor of the empty resonator. We should emphasise that the absorption dip looks a bit asymmetric, despite adjusting the set-up. This can be seen in the distance of the resonance position  $x_0$  and the bandwidth positions  $x_{l/r}$  in table I.

#### Calibration of the Hall probe

Before any productive measurements can be performed we need to gauge the Hall probe of the magnetic field. We have to do this, because we vary the magnetic field by ramping the Hall voltage on the computer. At first the value of the Hall voltage and the actual value of the magnetic field are not related in an explicit quantitative way. To determine an isomorphism between the two mentioned quantities we record an ESR spectrum of the DPPH and fit its shape to a differential Lorentzian to obtain the maximum of the resonance (root of the fitted function). This will give us an estimate for the magnetic field as all microscopic quantities of DPPH have been studied thoroughly in previous experiments. The important property here is the Landé- $g$ -factor which was found to be [3]

$$g_{\text{DPPH}} = 2.0036. \quad (52)$$

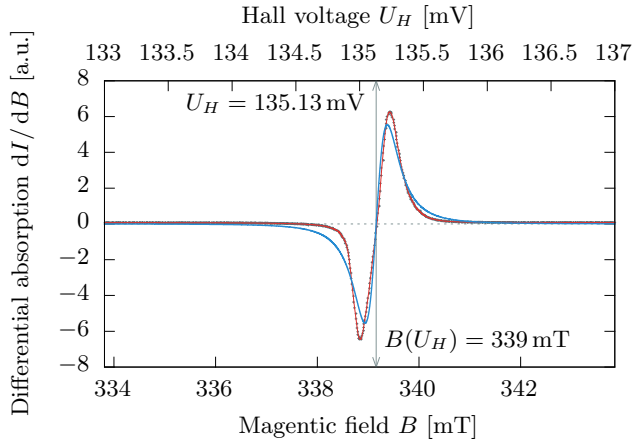
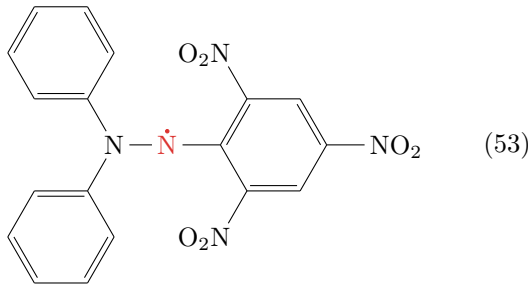


FIG. 5. First Measurement of the DPPH (poly) sample. This resonance spectrum gives use the magnetic field calibration for the following measurements.

The structure formula of 2,2-Diphenyl-1-Picrylhydrazyl (DPPH) reads



The main feature of DPPH is its stable free electron at the nitrogen atom, marked with a dot in the formula. This free electron is responsible for the ESR signal.

It is well known that there exists a linear dependence of the magnetic field on the Hall voltage. This proportionality factor is given by (27) and it follows

$$B(U_H) = \frac{h\nu_0}{g_{\text{DPPH}}\mu_B} \cdot \frac{U_H}{U_{\text{DPPH}}} \quad (54)$$

with Planck's constant  $h$ , the Bohr magneton  $\mu_B$  and the already mentioned Landé- $g$ -factor  $g_{\text{DPPH}}$ . The quantities  $U_{\text{DPPH}}$  and  $\nu_0$  have to be determined from the measurement. The resonance frequency  $\nu_0$  can be found in table I and is  $\nu_0 = 9.511$  GHz. From the fitted differential Lorentzian in figure 5 we find the maximum of the resonance, i.e., the root of the fit, at  $U_{\text{DPPH}} = 135.13$  mV.

Plugging in these values yields

$$B(U_H) = 2.5099 \cdot U_H. \quad (55)$$

In all figures the magnetic field is assigned to the lower  $x$ -axis and for reference the corresponding Hall voltage is always shown on the upper  $x$ -axis. In principle, the DPPH peak drifts during subsequent measurements due to thermal changes in the Hall probe. We didn't experience

this effect to have much influence and thus kept the existing calibration throughout all measurements.

Above we stated that we have obtained the value for the maximum of the resonance at  $U_{\text{DPPH}} = 135.13$  mV by finding the root of a differential Lorentzian fitted to the data. Here we present the ansatz function

$$\mathcal{F} = \frac{d\mathcal{L}}{dB} = -\frac{8I}{(\Delta B)^2} \frac{B - B_{\text{res}}}{\left[1 + \left(\frac{2}{\Delta B}(B - B_{\text{res}})\right)^2\right]^2}. \quad (56)$$

The fitting routine of the `gnuplot` utility provides the following values:  $I = -3.2424$  a.u.,  $\Delta B = 0.3029$  mV, and  $B_{\text{res}} = 135.13$  mV. After mapping these quantities using the conversion found above one has:  $\Delta B = 0.76018$  mV, and  $B_{\text{res}} = 339.158$  mV. We can compare  $B_{\text{res}} = 339.158$  mV to the analytical value described above  $B_{\text{DPPH}} = \frac{h\nu_0}{g_{\text{DPPH}}\mu_B} \approx 339.159$  mT.

#### Dependency of the spectra on different system parameters

To find a set of optimal system parameters it is useful to analyse the signal strength and its shape by varying:

- the modulation frequency, see figure 6,
- the integration time, see figure 7,
- the modulation amplitude, see figure 8,
- the power of the microwave, see figure 9.

From these figures we seek to find optimal parameters for further experiments. We will now discuss the results:

*Modulation Frequency:* All in all, five spectra for different modulation frequencies of the magnetic field were recorded in the range 2 kHz to 10 kHz. The measurement for 10 kHz was discarded, though, because the signal amplitude fell below any comparable order of magnitude and was only visible as a flat line in the comparative plot in figure 6.

In the figure the peaks were all slightly shifted to the right, thus the root of the curves does *not* correspond to the actual position of the resonance which is still at 339 mT.

The signal's amplitude decreases with increasing modulation frequency, whereas the curves becomes deformed for a frequency of 2 kHz. Nevertheless we will choose frequencies from the low regime for further measurement as these produce much stronger signals. For low frequency signals we observe a more visible scattering of data points around the spline.

We can say that for higher frequencies we obtain a smoother but weaker signal while for lower frequencies we obtain slightly noisy but more intense signals. Most of the spectra were recorded between 1 kHz and 2 kHz.

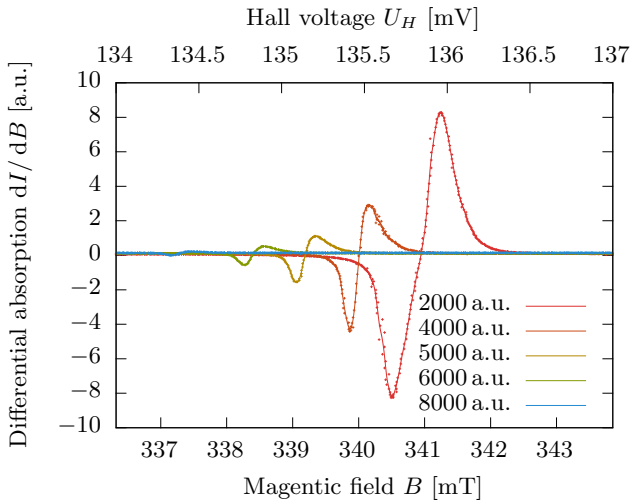


FIG. 6. Spectra of DPPH for different modulation frequencies  $\nu$ . The amplitude of the signal decreases with increasing frequency due to the increasing inductive reactance  $X_L = \omega L$  of the modulation coil. For better visibility the curves are overlaid with cubic splines and shifted in  $x$ -direction.

As an explanation for the drastic signal decay for high modulation frequencies we calculate the inductive resistance of the Helmholtz coils. This is given by

$$X_L = \omega L \quad (57)$$

and depends on the modulation frequency  $\omega_m$ . The magnetic field is determined by the current through the coils which is given by  $I = U/X_L \sim 1/\omega_m$ . This illustrates the inverse dependence and explains the decay which is then proportional to  $\nu^{-1}$ .

*Integration Time:* Several spectra of DPPH (poly) were recorded for different integration times of the lock-in amplifier. They are depicted in figure 7.

As above the curves were shifted in  $x$ -direction for better comparability. In a range from 1 ms to 100 ms the strength and shape of the signal are not affected by a change of  $\tau$ . Above the signal strength decreases and for  $\tau = 10\,000$  ms the shape is extremely deformed. The descending edge is damped more than the ascending side and is smeared out.

The deformation of the signal can be explained easily. On the computer the delay between two consecutive changes of the Hall voltage was set to 50 ms and wasn't altered throughout the whole experiment. If now the integration time is much larger than the delay between the Hall voltage changes one peak is averaged out and its amplitude is distributed to a broader range which is the mentioned smearing out. Another effect is that the averaging takes place over a negative and a positive peak both parts compensate each other and lead to a reduction of the signal strength.

The previous text might bring over the feeling that the averaging of the signal is a bad thing and destroys it.

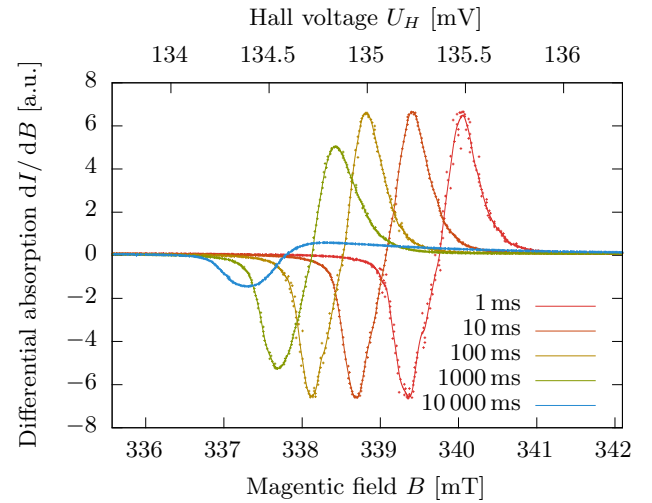


FIG. 7. Measurements of DPPH for different integration times  $\tau$  of the lock-in amplifier. For integration times higher than 100 ms the signal amplitude decreases and an asymmetry of the curve becomes visible. The data points were overlaid with a cubic spline. To compare the respective curves the spectrum is shifted in  $x$ -direction.

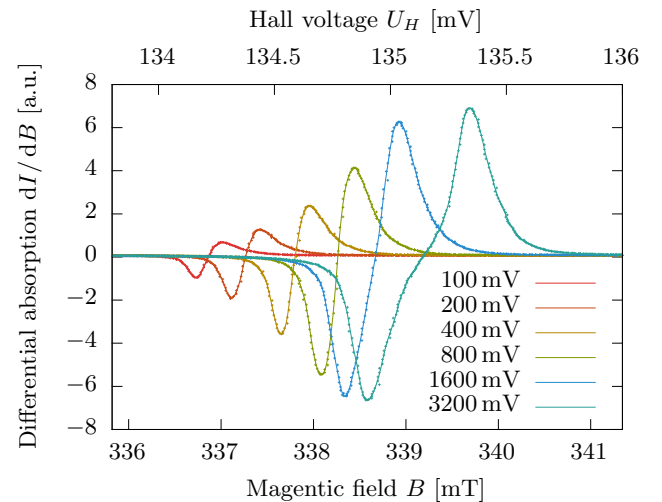


FIG. 8. Measurements of DPPH for different modulation amplitudes  $U$ . For amplitudes higher than 400 mV the curves deform and become asymmetric. The signal amplitude increases with increasing modulation amplitude. For better visibility the curves are overlaid with cubic splines and shifted in  $x$ -direction.

This is not entirely true because if we look at the curve for  $\tau = 1$  ms we can see scattering around the spline. To suppress this noise we need to average *a little* and thus we chose an integration time of  $\tau = 30$  ms for most of the measurements.

*Modulation Amplitude:* The ESR spectra of DPPH for different modulation amplitudes from 100 mV to 3200 mV are depicted in figure 8.

The figure shows that the modulation amplitude influ-

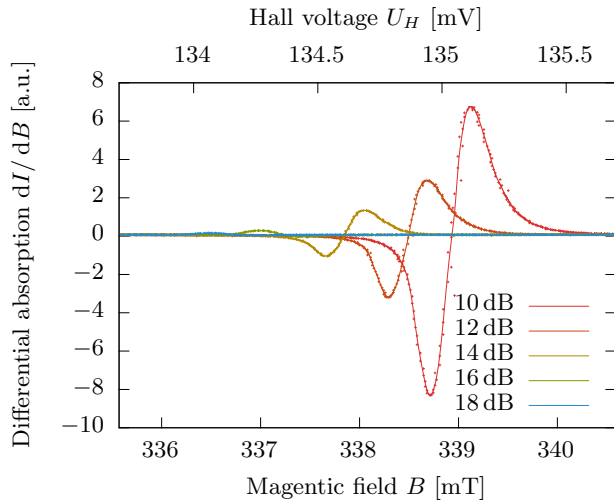


FIG. 9. Measurements of DPPH for different powers of the microwave. The higher the damping (in dB), which means with decreasing microwave power, the weaker the signal amplitude. The shape of the curve is not affected by varying the power. The data points were overlay with a cubic spline. To compare the respective curves the spectrum is shifted in  $x$ -direction.

ences the signal amplitude and the signal shape. In the area 100 mV to 400 mV the geometry of the curve remains unaffected while the signal amplitude increases. In ranges above 400 mV the signal amplitude saturates, the signal shape however becomes broader and asymmetric.

The separation of the two peaks for higher modulation amplitudes is a result of the vanishing intensity difference  $\Delta I = (dI/dB)\Delta B$  (see lock-in amplifier). Is the modulation amplitude from the same magnitude as the bandwidth of the resonance peak it is possible to measure at  $B_{\text{res}} - B_m$  the intensity  $I = 0$  and at  $B_{\text{res}} + B_m$  the intensity  $I \neq 0$  because we are on the resonance, consequently our peaks disperse.

The aim is to find a maximum modulation amplitude with minimum deformation of the signal shape. This is obvious for small modulation amplitudes the case, but the signal amplitude is still too weak for further measurements. As reasonable compromise we used the modulation amplitude 1000 mV.

*Microwave Power:* The DPPH spectra for different microwave powers in the range 10 dB to 18 dB are depicted in figure 9.

The figure shows a crucial impact of the microwave power on the signal amplitude. The higher the damping, which means a lower microwave power, the weaker the signal amplitude. Obviously low damping (i.e., high microwave powers) leads to high amplitudes. The signal shape is not affected by varying the damping. In summary it can be stated, that it is advisable to measure at high powers as long as the spectral lines are not getting broadened.

It should be noted, that the detector diode is limited,

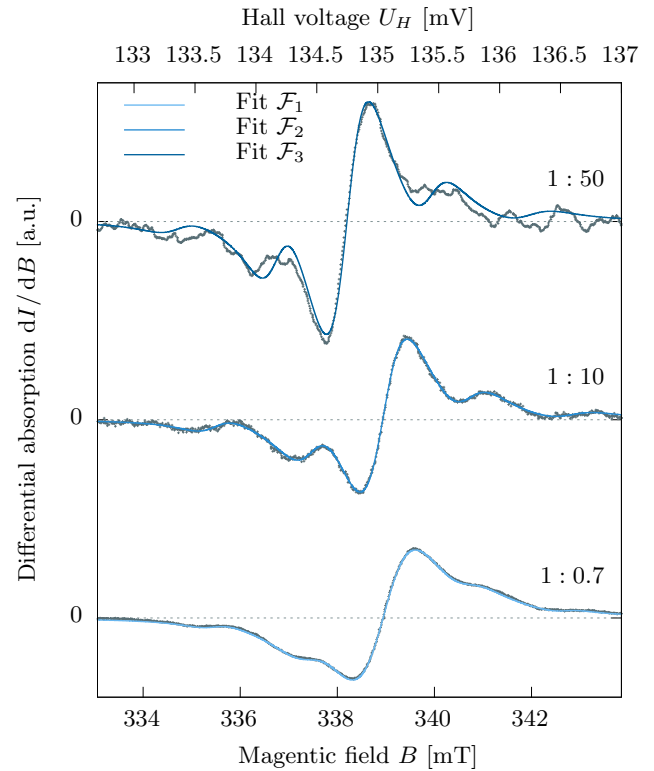


FIG. 10. Depicted are ESR spectra for different concentrations of DPPH in aqueous solution. The higher the concentration the better visible the hyperfine structure. One can observe all the five expected lines. For the highly dilute solution the signal is heavily distorted due to the lock-in amplifier, thus the function overlaid is only a “model” fit.

i.e., there is a technical limit to the microwave power, otherwise a destruction of the diode is possible.

### Hyperfine structure of DPPH

In the previous measurements we have been studying polycrystalline DPPH. This is handy to study all the properties found above, but to describe paramagnetic contributions to the spin diffusion the molecules need to have the ability to rotate in arbitrary directions. Thus, to observe the hyperfine structure of DPPH we record spectra for different concentrations in aqueous environment. The various spectra are depicted in figure 10.

For increasingly dilute DPPH solution the adjacent peaks get more and more accented, but also the signal strength decreases which is why it has to be amplified artificially and thus gets deformed. For small dilutions the neighbouring peaks are heavily damped away.

To determine the interesting parameters such as height, width and hyperfine splitting of the resonances we fit a superposition of five differential Lorentzians. The functional

form is given by

$$\mathcal{F} = \frac{d\mathcal{L}}{dB} = - \sum_{i=1}^5 \frac{8I_i}{(\Delta B_i)^2} \frac{B - B_{\text{res},i}}{\left[1 + \left(\frac{2}{\Delta B_i}(B - B_{\text{res},i})\right)^2\right]^2}. \quad (58)$$

where the parameter for the width is composed of several components

$$B_{\text{res},i} = \begin{cases} B_{\text{res}} + 2A_1 & \text{for } i = 1 \\ B_{\text{res}} + A_2 & \text{for } i = 2 \\ B_{\text{res}} & \text{for } i = 3 \\ B_{\text{res}} + A_4 & \text{for } i = 4 \\ B_{\text{res}} + 2A_5 & \text{for } i = 5 \end{cases} \quad (59)$$

This form helps us with the determination of the hyperfine splitting because these are now parameters of the fit. The fitted curves are overlaid with the data in figure 10. For the concentration 1 : 50 a “model” fit was imposed as one can see the data is not suited for good convergence, i.e. the fit parameters for this case are educated guesses based on the assumption that the width of the peaks and the hyperfine splitting should increase with decreasing concentration. The values were then augmented from the other two measurements. The height of the peaks was drawn by eye.

The values for the fit parameters are listed in table II. The width of the resonances and the hyperfine splitting were averaged over all five and four values, respectively. The approximate ratio of the intensity of the peaks can also be found there.

For the ratio of the intensities we expect 1 : 2 : 3 : 2 : 1. This is, unfortunately, in no way met. Because even the error has a huge scattering this has to be a systematic error and cannot be explained using a statistical argument. Even though the ratio is so far off we can still draw conclusions from it. For example we can definitely factor out that two resonances have the same height, thus the electron couples to at least two cores. Also, the fact that there are five resonances gives us  $2(I_1 + I_2) + 1 = 5$ , yielding  $I_1 = I_2 = 1$ . Thus the electron couples to the nitrogen atoms because these have a nuclear spin of  $I = 1$ .

For the value of hyperfine splitting we choose the results of the fit to the 1 : 10 sample as this possesses the best ratio of convergence of the fit and spectral line width. We average over the four values, because the hyperfine splitting should be equidistant for all resonances.

$$A_{\text{DPPH}} = 1.720 \text{ mT}$$

the hyperfine splitting of DPPH reaches from 1.12 mT to 1.73 mT as reported in [4]. This means that our values are within the range of possible results.

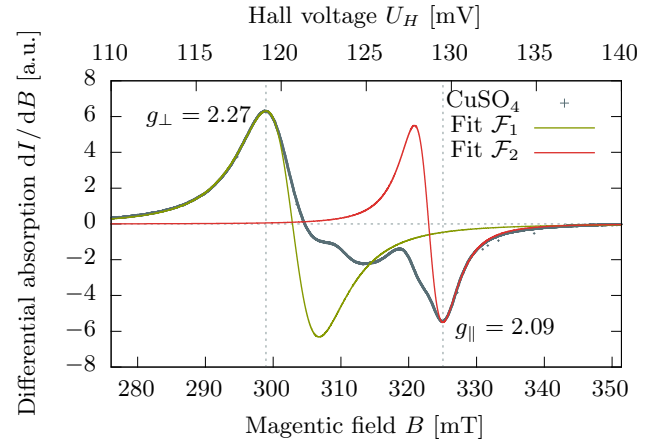


FIG. 11. ESR-spectrum of CuSO<sub>4</sub> with the two main values  $g_{\perp}$  and  $g_{\parallel}$  of the  $g$ -Tensor.

### $g$ -Tensor of Cu<sup>2+</sup>

Because of the crystalline structure of CuSO<sub>4</sub> the  $g$ -factor for the unpaired electron in Cu<sup>2+</sup> is anisotropic. As discussed in the basics the  $g$ -tensor can then be characterised by the eigenvalues  $g_{\perp}$  and  $g_{\parallel}$ . As a consequence we get an asymmetric broadened absorption spectrum (see figure 11). In the following discussion we want to determine  $g_{\perp}$  and  $g_{\parallel}$  with two methods. At first we present the method discussed in [5] and then the method discussed in [6].

*Method from [5]:* Like in [5] we can determine  $g_{\perp}$  and  $g_{\parallel}$  with the help of the peak positions. The calibration of the magnetic field gives us  $U_{\text{DPPH}} = 135.13 \text{ mV}$  and  $\nu_0 = 9.511 \text{ GHz}$ . With the well known  $g$ -factors of DPPH we find the connectivity

$$B(U_H) = 2.5099 \cdot U_H. \quad (60)$$

From figure 11 we can read out the magnetic fields to each peak. With help of the fundamental equation of ESR we get

$$\begin{aligned} B_{\perp} = 298.929 \text{ mT} & \implies g_{\perp} = \frac{h\nu}{B_{\perp}\mu_B} = 2.27, \\ B_{\parallel} = 325.049 \text{ mT} & \implies g_{\parallel} = \frac{h\nu}{B_{\parallel}\mu_B} = 2.09. \end{aligned}$$

The anisotropy of the crystal is characterised by the different  $g$ -values.

*Method from [6]:* According to the paper we can find the parameters  $g_{\alpha}$  and  $g_{\gamma}$  from a fit to the two partial peaks in the CuSO<sub>4</sub> · 5H<sub>2</sub>O ESR profile. To compute the desired  $g_{\perp}$  and  $g_{\parallel}$  from those we employ the mapping

$$\begin{aligned} g_{\alpha}^2 &= g_{\parallel}^2 \cos^2 \varphi + g_{\perp}^2 \sin^2 \varphi \\ g_{\gamma} &= g_{\perp} \end{aligned} \quad (61)$$

TABLE II. Listed below are the parameters of the fit (58) for the various concentrations of DPPH. In the last row of each table the estimated peak intensity ratio, the mean values of the FWHM, and the hyperfine splitting are presented. The centre of each resonance is given in the top row.

1 : 0.7 - $B_{\text{res}} = 338.96$ mT				1 : 10 - $B_{\text{res}} = 338.95$ mT				1 : 50 - $B_{\text{res}} = 338.20$ mT			
	$I_i$	$\Delta B_i$	$A_i$		$I_i$	$\Delta B_i$	$A_i$		$I_i$	$\Delta B_i$	$A_i$
	[a.u.]	[mT]	[mT]		[a.u.]	[mT]	[mT]		[a.u.]	[mT]	[mT]
1	-0.127	1.291	1.738	1	-0.366	1.461	1.728	1	-0.347	1.512	1.739
2	-0.749	1.757	1.474	2	-1.274	1.526	1.456	2	-1.709	1.319	1.448
3	-6.519	2.381	-	3	-5.816	1.794	-	3	-7.704	1.590	-
4	-0.472	1.676	1.712	4	-0.884	1.583	1.763	4	-1.397	1.474	1.718
5	-0.073	1.201	1.867	5	-0.288	1.896	1.933	5	-0.447	1.869	1.875
1:6:51:4:1			1.661 1.698	1:3:16:3:1			1.652 1.720	1:5:22:4:1			1.553 1.695

where  $\varphi = 41^\circ$  as extracted from table 1 in [6]. According to (27) we need the magnetic field at the level transition, which is the zeros of the differential profile (i.e., peaks of the intensity profile). These can be obtained from a fit to the two respective peaks and were extracted at the points  $B_{\text{res}}^\alpha = 302.851$  mT and  $B_{\text{res}}^\gamma = 322.947$  mT. With  $f_0 = 9.510$  GHz we obtain

$$g_\alpha = \frac{h\nu_0}{B_{\text{res}}^\alpha \mu_B} = 2.24 \quad (62)$$

$$g_\gamma = \frac{h\nu_0}{B_{\text{res}}^\gamma \mu_B} = 2.10 \quad (63)$$

Now we apply the mapping introduced above (61) to calculate the  $g$ -Tensor:

$$g_\perp = g_\gamma = 2.10 \quad (64)$$

$$g_\alpha = \sqrt{\frac{g_\alpha^2 - g_\perp^2 \sin^2 \varphi}{\cos^2 \varphi}} = 2.24 \quad (65)$$

Comparing this to the literature values in table 1 in [6]  $\hat{g}_\perp = 2.05$  and  $\hat{g}_\parallel = 2.38$  yields the relative deviations  $\mathcal{Q}(g_\perp, \hat{g}_\perp) = 2.4\%$  and  $\mathcal{Q}(g_\parallel, \hat{g}_\parallel) = 5.9\%$ . This is unfortunately not within the error range given in the paper. This might be due to the fact that we didn't recalibrate the magnetic again and the thermal drift kicked in.

### ESR analysis of $Mn^{2+}$

In this section we are going to determine the  $g$ -factor and the hyperfine structure of a liquid  $Mn^{2+}$  solution. Therefore an ESR spectrum was recorded and is depicted in figure 12.

For the subsequent calculations we need several parameters of the resonance spectrum. These include the peak intensity  $I$ , the zero  $B_{\text{res}}$  and the width  $\Delta B$ . For this specific case we fit a superposition of six differential

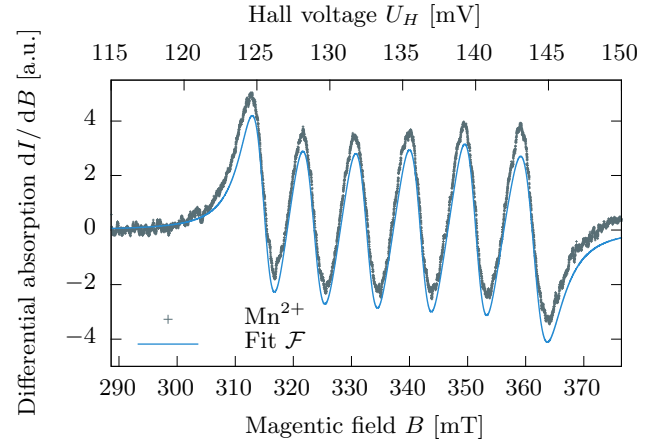


FIG. 12. In the ESR spectrum of  $Mn^{2+}$  the spin exchange is clearly visible as six distinct resonance peaks. The fitted function is a sum of six differential Lorentzians.

Lorentzians, given by

$$\mathcal{F} = \frac{d\mathcal{L}}{dB} = - \sum_{i=1}^6 \frac{8I_i}{(\Delta B_i)^2} \frac{B - B_{\text{res},i}}{\left[1 + \left(\frac{2}{\Delta B_i}(B - B_{\text{res},i})\right)^2\right]^2}. \quad (66)$$

The limit values of the several parameters are listed in table III.

As described in the previous text we need the resonance magnetic fields to compute the  $g$ -factor. In the formula of the  $g$ -factor there is in fact only one resonance value of the magnetic field. Thus the resonance value of the whole spectrum is approximated by the arithmetic mean over all six resonance values of the zeros (peaks). With the value from table III and  $f_0 = 9.518$  GHz one has

$$g = \frac{h\nu_0}{B_{\text{res}} \mu_B} = 2.01 \quad (67)$$

comparing that with the value found in [7]  $\hat{g} = 2.0025$  we have a relative deviation of  $\mathcal{Q}(g, \hat{g}) = 0.4\%$  which is really nice.

The hyperfine structure is given by the distance between

TABLE III. Listed below are the parameters of the fit (66). The ratio of the respective intensities, the arithmetic mean of the width, the resonance values, and the hyperfine splitting are listed in the last row of the table. These are needed for further calculations.

	$I_i$ [a.u.]	$\Delta B_i$ [mT]	$B_{\text{res},i}$ [mT]	$A_i$ [mT]
1	20.48	7.24	314.94	8.60
2	21.21	7.73	323.54	9.07
3	20.70	7.55	332.61	9.27
4	21.16	7.52	341.88	9.52
5	21.83	7.46	351.40	9.94
6	24.67	8.53	361.34	–
	1:1:1:1:1:1	7.67	337.62	9.28

adjacent absorption peaks, i.e., zeros of the differential absorption. In theory all of those should be the same. This is obviously not met as can easily be seen from table III. Thus we present the arithmetic mean of all those values as our hyperfine structure splitting.

$$A = 9.28 \text{ mT} \quad (68)$$

Here  $A_3$  can be compared to the literature value found in [8, p. 43]  $\hat{A}_3 = 8.69 \text{ mT}$  which yields a relative deviation of  $\mathcal{Q}(A_3, \hat{A}_3) = 6.7\%$ .

#### Spin Density at the Core

The hyperfine splitting is readily connected with the Fermi contact interaction. It describes the spin-spin coupling of the electron and the core at the position of the core. Hence we can calculate the probability of presence of the electron at the core using the measured values of the hyperfine splitting of DPPH and  $\text{Mn}^{2+}$ . The term spin density is not chosen very wisely in this context as it does not describe a spacial density of “matter”, but a probability density of presence of *one* particle at the core. This is denoted by  $|\psi(0)|^2$ . The formula for this quantity is taken from [9].

$$|\psi(0)|^2 = \frac{3}{2} \frac{A}{\mu_0 g_I \mu_K} \quad (69)$$

with the Landé-factor  $g_I$  of the core, the core magneton  $\mu_K$  and the magnetic field constant  $\mu_0$ .

With the values from the previous text we can determine the spin density for DPPH and  $\text{Mn}^{2+}$ . As a reminder, the values are

$$A_{\text{DPPH}} = 1.72 \text{ mT} \quad (70)$$

$$A_{\text{Mn}^{2+}} = 9.28 \text{ mT} \quad (71)$$

Plugging these into the formula for the spin density, together with the constants  $g_{I,\text{DPPH}} = 0.4038$  and

$g_{I,\text{Mn}^{2+}} = 1.3819$  one has:

$$|\psi_{\text{DPPH}}(0)|^2 = 1.007 \cdot 10^{30} \text{ m}^{-3}, \quad (72)$$

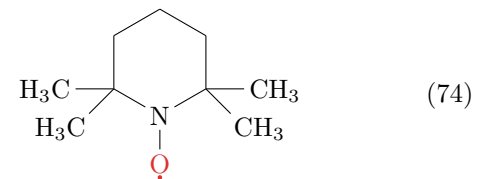
$$|\psi_{\text{Mn}^{2+}}(0)|^2 = 1.587 \cdot 10^{30} \text{ m}^{-3}. \quad (73)$$

In the case of  $\text{Mn}^{2+}$  the paramagnetic electrons are in the  $d$  orbital and hence the presence of the electrons at the core is zero. Consequently the Fermi contact interaction is in this case not possible (only for  $s$  electrons). For electrons in the  $p$ ,  $d$ ,  $f, \dots$ -orbitals the dipole-dipole interaction of the electrons and the nuclear moments is responsible for the hyperfine splitting and the not vanishing value of  $|\psi_{\text{Mn}^{2+}}(0)|^2$  [9].

## Experiments on ESR II

In the present section we seek to study the spin exchange in TEMPO and its impact on the form of the spectral lines in an ESR spectrum. We are going to quantify the spin diffusion by analysing the line widths of the hyperfine splitting.

The substance in use is TEMPO, which is an acronym for (2,2,6,6-Tetramethylpiperidin-1-yl)oxyl. The structure formula reads



The unpaired electron of the oxygen is responsible for the ESR signal. ESR spectra are recorded for different concentrations of TEMPO in toluene solution ranging from  $0.25 \text{ mmol l}^{-1}$  to  $250 \text{ mmol l}^{-1}$ . As O has a nuclear spin of  $I = 0$  the only coupling for the electron is possibly to the adjacent N core with nuclear spin  $I = 1$ . Thus  $2 \cdot 1 + 1 = 3$  hyperfine peaks can be observed.

#### Dependency of the spectra on the TEMPO concentration

Visibility and line width of the hyperfine splitting is critically dependent on the spin exchange rate, which in turn is dependent on the concentration of the ESR active substance. A plot of all measurements for varying concentration are shown in figure 13 in a waterfall plot. It is visible that for decreasing concentration the amplitude drops but also for  $c \leq 25 \text{ mmol l}^{-1}$  we find three resonance peaks of approximately same height.

From these observations we feel confident to draw the following conclusions:

- *Slow Spin Exchange:* For concentrations in the range of  $0.25 \text{ mmol l}^{-1}$  to  $25 \text{ mmol l}^{-1}$  we can see

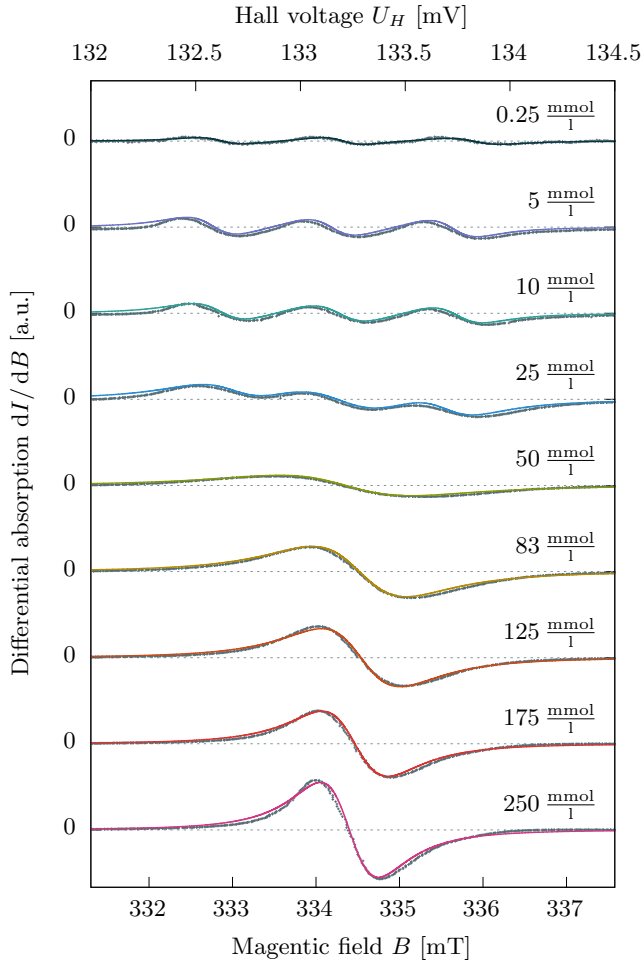


FIG. 13. Depicted is a series of several measurements with varying concentration of the TEMPO solution. The coloured curves are fits. With increasing concentration the hyper fine splitting broadens and finally coalesces into one peak at  $c = 50 \text{ mmol l}^{-1}$ . The spin exchange results in a narrowing of the left over resonance. The intensity of the curves with lower concentration was scaled up logarithmically with respect to the one for  $250 \text{ mmol l}^{-1}$ , because otherwise one would only see flat lines for these.

three distinct peaks, i.e. three possible hyperfine transitions. This is due to the fact that the spin exchange is slow compared to transition times.

- *Moderate Spin Exchange:* For a concentration of  $50 \text{ mmol l}^{-1}$  the spin exchange is slightly faster and leads to a unification of the distinct peaks. They are now incorporated in one wide peak.
- *Fast Spin Exchange:* For concentrations  $83 \text{ mmol l}^{-1}$  to  $250 \text{ mmol l}^{-1}$  the one remaining peak gets more and more accented. The system is now fully described by only one transition and the narrower the peak the smaller the time-energy uncertainty.

TABLE IV. Line width of the hyperfine resonances extracted from the ESR spectra in figure 13. For faster spin exchange there is only one peak, thus only one line width.

$c$ [mmol l <sup>-1</sup> ]	$\Delta B_1$ [mT]	$\Delta B_2$ [mT]	$\Delta B_3$ [mT]	$\langle \Delta B_i \rangle$ [mT]
0.25	0.950	0.895	1.100	0.982
5	1.094	1.076	1.046	1.072
10	1.172	1.220	1.118	1.170
25	1.576	2.097	1.400	1.691
50	–	2.712	–	2.712
83	–	1.940	–	1.940
125	–	1.629	–	1.629
175	–	1.364	–	1.364
250	–	1.202	–	1.202

#### Analysis of the Spin Exchange

To study the dependency of the spin exchange on the TEMPO concentration we plot the line widths over the concentration. The rate constant  $k_e$  of the spin exchange can then be extracted from fits to the data.

First of all we need to extract the line width of the resonance peaks from the fits in figure 13. Therefore differential Lorentzians were fitted to the data.

$$\mathcal{F} = \frac{d\mathcal{L}}{dB} = -\frac{8I}{(\Delta B)^2} \frac{B - B_{\text{res}}}{\left[1 + \left(\frac{2}{\Delta B}(B - B_{\text{res}})\right)^2\right]^2}. \quad (75)$$

For the curves with three peaks, i.e.,  $0.25 \text{ mmol l}^{-1}$  to  $25 \text{ mmol l}^{-1}$ , a superposition of three fits was chosen.

$$\mathcal{G} = \frac{d\mathcal{L}}{dB} = -\sum_{i=1}^3 \frac{8I_i}{(\Delta B_i)^2} \frac{B - B_{\text{res},i}}{\left[1 + \left(\frac{2}{\Delta B_i}(B - B_{\text{res},i})\right)^2\right]^2}. \quad (76)$$

The fit parameters obtained from `gnuplot` are listed in table IV.

According to theory all line width should be the same for the spectra with three peaks which they are almost in a first approximation. Still, to eliminate errors we average over the values. The so obtained values are plotted over their corresponding concentration to achieve figure 14. The values for slow spin exchange are highlighted with a grey background. Even without the additional fit curves one can clearly see that the values for slow spin exchange are neatly aligned on an ascending slope, whereas the values for moderate and fast spin exchange obviously decay (it cannot be told at first sight if this is a power law or an exponential).

In the basics, as in [10], a linear dependency between concentration and line width was found for slow spin exchange.

$$k_e c = \frac{g_e \mu_B}{\hbar} \left| \frac{1}{1 - \varphi} \right| (\Delta B(c) - \Delta B(0)) \quad (77)$$

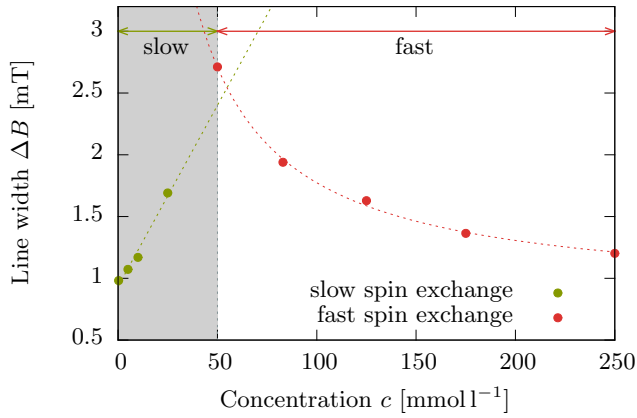


FIG. 14. Plotted is the average line width of the hyperfine resonances  $\Delta B$  over the concentration of TEMPO  $c$ . The data of this plot can be reviewed in table IV.

For equally distributed intensities to all peaks one has  $\varphi = 1/3$ . Furthermore it is given that  $g_e = g_{\text{TEMPO}} = 2.0058$ . To obtain  $k_e$  we fit a linear slope to the values for the slow spin exchange.

$$\mathcal{F}_{k_e}(c) = \alpha \cdot c + \beta \quad (78)$$

Using the `gnuplot` utility we find the values  $\alpha = 0.0293$  and  $\beta = 0.934$ . While we are not really interested in  $\beta$ , we are definitely interested  $\alpha$ , as this is proportional to our rate constant. Together with the above relations one has

$$k_e = \frac{g_e \mu_B}{\hbar} \left| \frac{1}{1 - \varphi} \right| \alpha = 7.773 \cdot 10^9 \text{ l mol}^{-1} \text{ s}^{-1} \quad (79)$$

Unfortunately [10] doesn't list any values for our experimental configuration. However [11] lists some values for pretty similar setups:

$$\begin{aligned} \text{TEMPO in acetone: } & k_e = 7.8 \cdot 10^9 \text{ l mol}^{-1} \text{ s}^{-1} \\ \text{TEMPO in methanol: } & k_e = 2.8 \cdot 10^9 \text{ l mol}^{-1} \text{ s}^{-1} \\ \text{4-oxo-TEMPO in acetone: } & k_e = 8.1 \cdot 10^9 \text{ l mol}^{-1} \text{ s}^{-1} \\ \text{4-oxo-TEMPO in toluene: } & k_e = 5.27 \cdot 10^9 \text{ l mol}^{-1} \text{ s}^{-1} \end{aligned} \quad (80)$$

Our values stand in good agreement with these. Thus we consider our analysis correct.

For the fit for the data for the fast spin exchange we assumed a power law given by

$$\mathcal{G}_{k_e}(c) = \frac{\xi}{c} + \zeta \quad (81)$$

This form yields a good overlap with the data points. The parameters obtained using `gnuplot` are  $\xi = 93.50$  and  $\zeta = 0.839$ .

### Lifetime of the Spin States

One method to describe states of finite lifetime is non-hermitian quantum mechanics (NHQM) [12]. This theory stands out due to the fact, that in contrast to normal quantum mechanics the Hamiltonian does not need to be hermitian, i.e.,  $H \neq H^\dagger$ . Those non-hermitian operators possess eigenvalues which are in general complex. Looking at the unitary time evolution of a state

$$\psi(t) = e^{-i\lambda t/\hbar} \psi(t_0) \quad (82)$$

one immediately sees that an imaginary part in  $\lambda$  is equivalent to a decay rate. States with an eigenvalue with an imaginary part not equal to zero are called resonances. For a general resonance one assumes

$$\lambda = E - i\frac{\Gamma}{2} \quad (83)$$

with the decay rate  $\Gamma$  of the resonance. As the unitary time evolution is no longer norm conserving a new form of the measurement postulate needs to be found

$$P_i = \langle \phi_i | \psi \rangle \langle \tilde{\psi} | \chi_i \rangle \quad (84)$$

with the left eigenvector  $\langle \phi_i |$ , the right eigenvector  $|\chi_i\rangle$  and the dual conjugate state  $\langle \tilde{\psi} |$ . The decay rate  $\Gamma$  can be seen as the line width of the state in units of energy and we define the lifetime  $\tau = \hbar/\Gamma$ .

In our example the line width is given by  $\Delta B$  which is connected to energy via equation (27). Using this in the definition of the lifetime, one has

$$\tau = \frac{\hbar}{g_e \mu_B \Delta B} \quad (85)$$

Plugging in the data from table IV yields the plot in figure 15.

The lifetime  $\tau$  of the hyperfine states increases for decreasing concentration in the regime of the fast spin exchange. For the regime of the slow spin exchange the case is exactly vice versa, the lifetime  $\tau$  of the hyperfine states decreases for increasing concentration.

### SUMMARY

In the following section we want to summarise the experimental results. Note that thanks to the damaged klystron a analysis of the first lab day (experiments with microwaves) was not possible.

#### Experiments on ESR I

*Quality of the resonator:* With help of equation  $Q = \nu_0/\Delta\nu$  we determined the quality factors  $Q$  for an empty resonator and a filled one. The particular  $Q$ -factors are listed in table I.

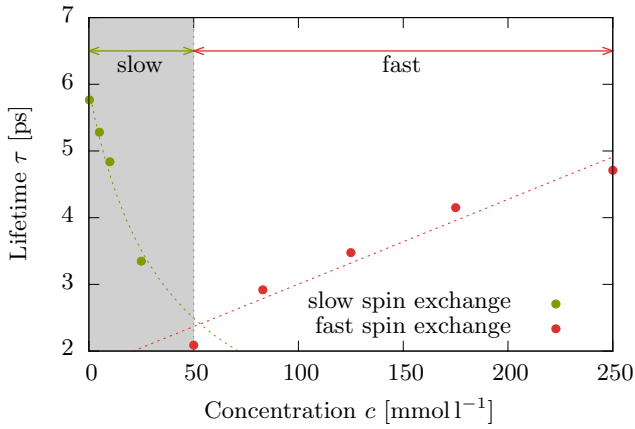


FIG. 15. Plotted is the lifetime of the spin states  $\tau$ , as obtained from their line widths, over the concentration of TEMPO  $c$ . For the slow spin exchange we find the expected behaviour, verified by a fit. For the fast spin exchange the expectation is broken as the data is not aligned on a fit of the expected behaviour.

*Calibration of the Hall probe:* With the well known  $g$ -factor of DPPH and the measured microwave frequencies we were able to find the relation

$$B(U_H) = 2.5099 \cdot U_H \quad (86)$$

for the calibration of the magnetic field.

*Dependency of the spectra:* In this task we investigated the behaviour of the ESR spectra of DPPH depending on different system parameters (modulation frequency, integration time, modulation amplitude and power of the microwave). Due to the inductive reactance of the modulation coil the signal amplitude decreased for high frequencies (see figure 6). Also for long integration times we observed asymmetric curves with decreasing amplitude (see figure 7). Depending on the modulation amplitude the signal became asymmetric. This was especially the case for high signal amplitudes (see figure 8). Varying the power of the microwave did not affect the shape of the curve (see figure 9).

*Hyperfine structure of DPPH:* For three DPPH samples of different concentrations we measured the ESR spectrum and determined the FWHM

$$\Delta B(1 : 0.7) = 1.661 \text{ mT} \quad (87)$$

$$\Delta B(1 : 10) = 1.652 \text{ mT} \quad (88)$$

$$\Delta B(1 : 50) = 1.553 \text{ mT}. \quad (89)$$

The ESR spectra, depicted in figure 10, show that only for highly diluted solutions it was possible to observe the hyperfine structure. The hyperfine splitting, caused by the nuclear spin  $I = 1$  was determined as

$$A_{\text{DPPH}} = 1.720 \text{ mT}, \quad (90)$$

which is within the range of possible results.

*$g$ -Tensor of  $\text{Cu}^{2+}$ :* Based on the ESR spectra of  $\text{CuSO}_4$ , depicted in figure 11, we used two methods to determine the parallel and perpendicular components of the  $g$ -Tensor. With the method, shown in [5] we found

$$g_{\perp} = 2.27 \quad \text{and} \quad g_{\parallel} = 2.09. \quad (91)$$

The method presented in [6] gives

$$g_{\perp} = 2.10 \quad \text{and} \quad g_{\parallel} = 2, 24. \quad (92)$$

Comparing this with the literature values  $\hat{g}_{\perp} = 2.05$  and  $\hat{g}_{\parallel} = 2.38$  yields the relative deviations

$$\mathcal{Q}(g_{\perp}, \hat{g}_{\perp}) = 2.4\% \quad \text{and} \quad \mathcal{Q}(g_{\parallel}, \hat{g}_{\parallel}) = 5.0\%. \quad (93)$$

Obviously, both methods yield different values.

*ESR analysis of  $\text{Mn}^{2+}$ :* Figure 12 shows the ESR spectrum of  $\text{Mn}^{2+}$ . The six visible peaks correspond to a hyperfine splitting in six lines. With help of the fit function (66) it was possible to determine the  $g$ -factor and the hyperfine splitting

$$g = 2.01, \quad (94)$$

$$A = 9.28 \text{ mT}. \quad (95)$$

The six hyperfine splittings indicate the nuclear spin  $I = 5/2$ .

*Spin density at the core:* With help of the previous hyperfine splitting it is possible to determine the spin density of the paramagnetic electrons for DPPH and  $\text{Mn}^{2+}$

$$|\psi_{\text{DPPH}}(0)|^2 = 1.007 \cdot 10^{30} \text{ m}^{-3} \quad (96)$$

$$|\psi_{\text{Mn}^{2+}}(0)|^2 = 1.587 \cdot 10^{30} \text{ m}^{-3}. \quad (97)$$

The spin density describes the probability density of presence of one particle at the core and not a spacial density of "matter". Note that here we have to deal with the Fermi contact interaction and the indirect hyperfine splitting due to the dipole-dipole interaction of the electrons and nuclear moments. The dipole-dipole interaction also leads to a hyperfine splitting of the unpaired electrons. For  $\text{Mn}^{2+}$  this is the case.

## Experiments on ESR II

*TEMPO concentration:* In figure 13 we see a series of ESR spectra with varying concentration of the TEMPO solution. Based on this figure we aim to investigate the spin exchange of the paramagnetic molecules. For concentrations 0.25 mmol/l to 25 mmol/l we are in the range of slow spin exchange. For a concentration of 50 mmol/l we are in the regime of moderate spin exchange. For concentrations 83 mmol/l to 250 mmol/l we are in the range of fast spin exchange.

*Spin Exchange:* Next, we plotted the average line width of the hyperfine resonances over the concentrations of TEMPO to determine the rate constant  $k_e$ . With help of equation 77 and an additional linear fit we found

$$k_e = 7.773 \cdot 10^9 \text{ l mol}^{-1} \text{ s}^{-1}. \quad (98)$$

which is within the range of possible results.

*Lifetime of the Spin States:* In figure 15 the lifetime of the spin states is plotted over the concentration of TEMPO. With help of non-hermitian quantum mechanics (NHQM) we derived a term for the lifetime

$$\tau = \frac{\hbar}{g_e \mu_B \Delta B}. \quad (99)$$

The regime of slow spin exchange decreases from 6 ps to 2.5 ps and transfer to the regime of fast spin exchange. Hence the lifetime  $\tau$  decreases with increasing concentration and vice versa for increasing  $\tau$ .

## APPENDIX

In this section you will find some formulas used in the report which were not explained in the basics, because they are not related to ESR in any way. Furthermore you may find comments on particular aspects of the report which are not of scientific nature.

*Arithmetic Mean:* The arithmetic mean of a series is defined as a sum over all members of the series divided by the number of members. Let  $s = \{s_i \mid 1 < i < N\}$ , then the arithmetic mean is given by

$$\bar{s} \equiv \frac{1}{N} \sum_{i=1}^N s_i. \quad (100)$$

*Relative Deviation:* The relative deviation is a measure for the difference between two values and is given in percent. Suppose  $a$  and  $b$  are measured values for the same quantity and thus have the same unit. Their relative deviation is given by

$$\mathcal{Q}(a, b) = \frac{a - b}{b} \cdot 100\%. \quad (101)$$

*Constants:* If not stated otherwise physical constants are taken from [13].

- [3] J. Davies, B. Gilbert, K. McLauchlan, and S. Eaton, *Electron Paramagnetic Resonance*, Specialist Periodical Reports (Royal Society of Chemistry, 2000).
- [4] R. W. Holmberg, *A Paramagnetic Resonance Study of Hyperfine Interactions in Single Crystals Containing  $\alpha, \alpha$ -diphenyl- $\beta$ -picrylhydrazyl.*, Tech. Rep. W-740.5-eng-26 (Oak Ridge National Laboratories, 1961).
- [5] F. K. Kneubühl, *The Journal of Chemical Physics* **33**, 1074 (1960).
- [6] R. D. Arnold and A. F. Kip, *Phys. Rev.* **75**, 1199 (1949).
- [7] L. Turyanska, R. J. A. Hill, O. Makarovsky, F. Moro, A. N. Knott, O. J. Larkin, A. Patane, A. Meaney, P. C. M. Christianen, M. W. Fay, and R. J. Curry, *Nanoscale* **6**, 8919 (2014).
- [8] M. Zimmerman and N. Whitehead, *New Applications of Electron Spin Resonance: Dating, Dosimetry and Microscopy* (World Scientific, 1993).
- [9] H. Haken and H. C. Wolf, *Molekülphysik und Quantenchemie*, 5th ed. (Springer Verlag, 2005).
- [10] Y. Molin, K. Salikhov, and K. Zamaraev, *Spin Exchange: Principles and Applications in Chemistry and Biology*, Springer Series in Chemical Physics (Springer Berlin Heidelberg, 2012).
- [11] G. Grapp and K. Rasmussen, *Nitroxides – Theory, Experiment and Applications*, (2012), 10.5772/39131.
- [12] N. Moiseyev, *Non-Hermitian Quantum Mechanics* (Cambridge University Press, 2011).
- [13] P. J. Mohr, B. N. Taylor, and D. B. Newell, *Rev. Mod. Phys.* **84**, 1527 (2012).

---

\* Michael.1233@gmx.de

† henrimenke@gmail.com

[1] D. Meschede, *Gerthsen Physik*, 24th ed. (Springer Verlag, 2007).

[2] W. Balter and L. W. Kroh, *Schnellmethoden zur Beurteilung von Lebensmitteln und ihren Rohstoffen* (Behr, 2004).